Graph Structural Descriptors for Classification of Soybean Grains

Eduardo da Silva Afonso
Institute of Math. & Computer Science
University of São Paulo
São Carlos, Brazil
eduardo.afonso@usp.br

Jianglong Yan
Institute of Math. & Computer Science
University of São Paulo
São Carlos, Brazil
jianglong@usp.br

Murillo G. Carneiro
Faculty of Computing
Federal University of Uberlândia
Uberlândia, Brazil
mgcarneiro@ufu.br

Kaizhou Gao
Faculty of Innovation Engineering
Macau University Sci. & Tech.
Macau, China
kzgao@must.edu.mo

Huaqiang Yuan
School of Computer Sci. and Tech.
Dongguan University of Technology
Dongguan, China
yuanhq@dgut.edu.cn

Liang Zhao
Faculty of Philosophy, Sciences and Letters
University of São Paulo
Ribeirão Preto, Brazil
zhao@usp.br

***Abstract*—The soybean production chain continues to face important technical and operational challenges, among which automatic grain quality classification remains a major concern. Although deep learning techniques have been extensively employed for soybean grain classification and related agricultural tasks, they still exhibit key practical limitations. These include dependence on large annotated datasets, limited sensitivity to subtle damage patterns, reduced interpretability, and considerable computational cost. To mitigate these issues, we propose a graph construction strategy based on images that encodes rich visual cues, namely color, texture, and curvature, from segmented image regions. On top of this representation, we develop a classification approach for soybean grain images using graph-derived features. By modeling structural relationships in the data instead of depending exclusively on pixel-level detail, the proposed method is able to achieve strong classification results even with a limited amount of training data. The experimental findings also indicate that the inclusion of graph-based features extracted from soybean images leads to clear improvements in classification accuracy.**

***Index Terms*—Soybean grain classification, soybean quality control, graph metrics, graph feature descriptors, pattern-based learning, deep learning**

I. INTRODUCTION

Soybean (*Glycine max*) plays a central role in the global agricultural economy and is among the most important crops worldwide in terms of production volume and trade [1]. Despite its economic relevance, the soybean supply chain still faces technical challenges in quality control of harvested grains. Traditionally, quality assessment relies on manual visual inspection, which is time-consuming, subjective, and prone to human error in large-scale operations. Common visual defects include immature, broken, spotted, or skin-damaged grains, which affect market value and industrial processing efficiency.

To overcome the limitations of manual inspection, automatic grain quality assessment has become a priority. Convolutional neural networks (CNNs) have shown strong performance in soybean grain inspection tasks [2], [3]. However, standard CNN architectures may incur high computational costs and large parameter counts, which can hinder deployment in real-time or resource-constrained environments [4]. Although lightweight architectures mitigate complexity, they may still face trade-offs in accuracy for subtle defect classes. Other strategies include spectroscopy-based analysis and object detection variants for soybean assessment [5], [6]. Despite their effectiveness, these approaches commonly require large labeled datasets, architecture-specific tuning, and provide limited interpretability.

These limitations motivate alternative representations that capture structural information beyond fine-grained pixel-level features. In this context, graph-based models offer a promising framework for representing images, encoding relationships between image components (e.g., pixels, superpixels, or segmented regions) as nodes and edges. Such representations can emphasize structural patterns and improve robustness to noise and geometric variations. Prior works have demonstrated the potential of graph-based modeling for visual analysis tasks, including texture classification and segmentation [7], [8].

This work proposes a methodology for classifying soybean grain images using structural features extracted from graphs constructed from the original images. Each image is segmented into meaningful regions mapped to graph nodes, while edges are defined using similarity measures derived from color, texture, and curvature. Graph-derived descriptors are then integrated into the classification pipeline to enhance performance under limited training data.

This work presents the following contributions:

- We propose an image classification method that leverages graph-based features to capture structural patterns, achieving strong performance with a small training set.
- We introduce an image-based graph construction method in which each node corresponds to an image segment

and edges encode similarity based on color, texture, and curvature cues.
- We combine complementary graph descriptors and apply feature selection to improve efficiency and classification accuracy.
- We show that integrating graph-based features with CNN representations improves classification performance compared to image-only baselines.

II. Materials and Methods

This section presents the proposed methodology for soybean seed classification using graph representations derived from image data. The overall pipeline is illustrated in Figure 1, which outlines each stage of the process from raw image input to final classification output.

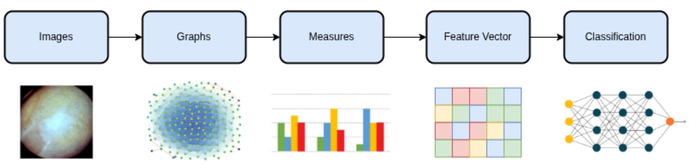

Fig. 1: Methodological pipeline: from images to classification.

The full pipeline is divided into five main steps, beginning with dataset description and followed by image preprocessing, graph construction, feature extraction, and classification.

A. Image Preprocessing and Segmentation

The image preprocessing pipeline included the following steps:

- **Resizing**: All images were resized to a uniform size of 227×227 pixels.
- **Dark Region Filtering**: Low-intensity regions, particularly at the image corners, were removed to eliminate non-informative background artifacts.

The segmentation is performed using the *Simple Linear Iterative Clustering - SLIC* algorithm [9], which groups adjacent pixels based on color similarity and spatial proximity, forming so-called *superpixels*. Each superpixel is represented as a node in the graph.

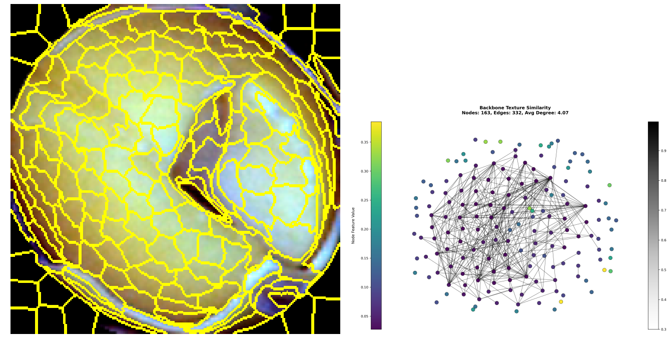

(a) (b)

Fig. 2: (a) Illustration of a *Broken* soybean grain image and its segmentation result. (b) The corresponding graph constructed based on texture similarity. Each segment in (a) is a node of the graph in (b).

The distance metric between a pixel and the cluster center is defined as:

$$D = \sqrt{d_c^2 + \left(\frac{d_s}{S}\right)^2 m^2} \quad (1)$$

where:

- d_c is the color distance: $d_c = \sqrt{(l_i - l_k)^2 + (a_i - a_k)^2 + (b_i - b_k)^2}$
- d_s is the spatial distance: $d_s = \sqrt{(x_i - x_k)^2 + (y_i - y_k)^2}$
- $S = \sqrt{H \cdot W / N_s}$ is the expected average size of super-pixels
- m is the compactness parameter

Figure 2 (a) show example a Broken grain image and their corresponding segmentation results.

B. Image Graph Construction

After each image is segmented using the SLIC algorithm, each segment s_i is turned out to be a node of the graph: $S = \{s_1, s_2, ..., s_N\}$, which is associated with a feature vector $\mathbf{x}_i$ composed of:

- Mean RGB components: μ_R, μ_G, μ_B
- Texture descriptors (gradient magnitude)
- Curvature descriptors (from second-order gradients)

To construct graph representations from the segmented images, each superpixel is encoded by a feature descriptor that captures local visual information. Considering separately the RGB components, texture, and curvature, five distinct graphs are generated—each encoding one type of visual attribute. The descriptors [10], [11] are computed as follows:

- **Color descriptor:** Each region M_i has its mean color calculated in the RGB channels:

$$c_i = \left[\frac{\text{mean}(I[M_i, 0])}{255}, \frac{\text{mean}(I[M_i, 1])}{255}, \frac{\text{mean}(I[M_i, 2])}{255}\right] \quad (2)$$

- **Texture descriptor:** For each channel $s \in \{0, 1, 2\}$, the gradient magnitude G_s is calculated and normalized:

$$G_s = \sqrt{G_{x,s}^2 + G_{y,s}^2}, \quad \text{normalized} \tag{3}$$

$$G_s = \frac{G_s - \min(G_s)}{\max(G_s) - \min(G_s)} \tag{4}$$

The texture descriptor for region M_i is given by the average gradient across all channels:

$$t_i = \frac{1}{3} \sum_s \text{mean}(G_s[M_i]) \tag{5}$$

- **Curvature descriptor:** First, the normalized gradients are computed:

$$\hat{G}_x = \frac{G_x}{\sqrt{G_x^2 + G_y^2 + 10^{-10}}}, \quad \hat{G}_y = \frac{G_y}{\sqrt{G_x^2 + G_y^2 + 10^{-10}}} \tag{6}$$

Then, the curvature is defined as:

$$\kappa = \left| \frac{\partial \hat{G}_x}{\partial x} + \frac{\partial \hat{G}_y}{\partial y} \right|, \quad \kappa_i = \text{mean}(\kappa[M_i]) \tag{7}$$

Once each region M_i is described by its corresponding feature vector (color c_i, texture t_i, or curvature κ_i), graphs are built by connecting node pairs (v_i, v_j) whose regions exhibit visual similarity. The edge weights are computed using the following similarity functions:

- **Color Similarity (RGB):**

$$\text{sim}_c(v_i, v_j) = 1 - \frac{\|c_i - c_j\|_2}{\sqrt{3}} \tag{8}$$

- **Texture Similarity:**

$$\text{sim}_t(v_i, v_j) = \frac{t_i \cdot t_j}{\|t_i\|_2 \cdot \|t_j\|_2} \tag{9}$$

- **Curvature Similarity:**

$$\text{sim}_\kappa(v_i, v_j) = 1 - |\kappa_i - \kappa_j| \tag{10}$$

These similarity functions ensure that the resulting graphs encode not only the local features of each superpixel but also the structural relationships between visually similar regions, enabling subsequent analysis using graph-theoretic and learning-based methods.

In this way, the five graphs generated from this approach are:

- Red Channel Graph (G_R): based on red intensity values
- Green Channel Graph (G_G): based on green intensity values
- Blue Channel Graph (G_B): based on blue intensity values
- Texture Graph (G_T): based on gradient-based features
- Curvature Graph (G_C): based on border geometry and morphological characteristics

To ensure the connectivity of each graph, a minimum spanning tree (MST) is applied when disconnected components are present.

Figure 2(b) shows examples of the constructed texture graphs (G_T) of the image in Figure 2(a), respectively. The color variations highlight the qualitative differences in connection strength between the two graphs.

C. Graph Feature Extraction

From each graph G_R, G_G, G_B, G_T, and G_C, we extracted 10 commonly used topological metrics, including degree-based measures, shortest-path and centrality measures, clustering coefficient, modularity, and assortativity [12], [13]. This yields a feature vector $\mathbf{f}^{(k)} \in \mathbb{R}^{10}$ for each graph. The final image descriptor is obtained by concatenating the vectors:

$$\begin{aligned} \mathbf{f}^{(i)} = [&f_{WSD}, f_{SPL}, f_{WD}, f_{WDSD}, f_{WCC}, \\ &f_M, f_{WA}, f_{EC}, f_{CC}, f_{BC}], \quad i = 1, 2, ..., 5 \end{aligned} \tag{11}$$

$$\mathbf{F} = \left[\mathbf{f}^{(1)} \parallel \mathbf{f}^{(2)} \parallel \cdots \parallel \mathbf{f}^{(5)} \right] \tag{12}$$

Accordingly, each image is encoded as a 50-dimensional feature vector $\mathbf{F}$, formed by concatenating 10 topological metrics computed across 5 distinct graph representations ($5 \times 10 = 50$ measures). The five graph representations emphasize different aspects of the soybean seed's visual structure and serve as the basis for structural feature extraction.

D. Outlier Removal and Feature Selection

We employed a two-fold feature selection strategy combining ANOVA (Analysis of Variance) and Mutual Information to identify the 25 most relevant structural measures from the total 50 measures for classification. ANOVA evaluates whether the mean values of a given feature differ significantly across multiple classes. It does so by computing the F-statistic:

$$F = \frac{MS_{\text{between}}}{MS_{\text{within}}} = \frac{\frac{SS_{\text{between}}}{k-1}}{\frac{SS_{\text{within}}}{n-k}} \tag{13}$$

where:

- SS_{between} is the sum of squares between classes (explained variance),
- SS_{within} is the sum of squares within classes (residual variance),
- k is the number of classes, and
- n is the total number of samples.

A higher F value suggests a stronger association between the feature and the class labels. The statistical significance is evaluated via the associated p-value.

Complementarily, Mutual Information quantifies the statistical dependence between a feature X and the target class Y. It measures how much knowing the value of X reduces uncertainty about Y, and is defined as:

$$I(X; Y) = \sum_{x \in X} \sum_{y \in Y} p(x, y) \cdot \log \left(\frac{p(x, y)}{p(x)p(y)} \right) \tag{14}$$

where:

- $p(x, y)$ is the joint probability distribution of X and Y,

- $p(x)$ and $p(y)$ are their respective marginal distributions.

Mutual Information is non-negative and equals zero only when X and Y are statistically independent. High values indicate a strong dependency.

Each feature was ranked separately according to both criteria. The ranks were then summed to obtain a final score, and the 25 features with the lowest combined scores were selected. This hybrid strategy ensures that both linear separability (captured by ANOVA) and non-linear dependencies (captured by Mutual Information) are considered, improving the robustness and interpretability of the classification pipeline.

E. Classification

Classification is performed using convolutional neural networks (CNNs), specifically ResNet50 [14], InceptionV3 [15], and EfficientNet [16]. The dataset is randomly partitioned into training (80%), validation (10%), and test (10%) subsets. The models are trained using the Adam optimizer with a learning rate of 0.0001, and the loss function used is the cross-entropy loss. To improve convergence and generalization, a learning rate scheduler (`StepLR`) is applied, which decreases the learning rate by a factor of 0.1 every 7 epochs.

Beyond training baseline CNN models on raw image data, a hybrid strategy has been implemented to integrate topological information extracted from graph representations of the same images. Specifically, structural graphs are generated from five perspectives—RGB channels, texture, and curvature—and ten topological metrics are computed for each, resulting in a 50-dimensional feature vector. After feature selection, the most discriminative 25 features are used as the graph-based representation.

To integrate visual and structural features, the final classification layer of each CNN is removed and its penultimate feature vector is concatenated with the selected graph-based features. The combined vector is then fed into a lightweight classification head composed of fully connected layers with ReLU activation and dropout.

This hybrid fusion strategy is consistently applied to ResNet50, InceptionV3, and EfficientNet, enabling a direct comparison between image-only and graph-enhanced models. Performance is evaluated using accuracy, precision, recall, and F1-score under both multiclass and binary classification scenarios to assess the contribution of structural descriptors to discriminative performance.

III. Experimental Results

The experimental results presented below demonstrate the performance of classification models based on structural graph representations derived from soybean grain images. Tests are conducted using three different neural network architectures, covering both the complete five-class scenario (Intact, Spotted, Broken, Skin damaged, Immature) and two practical binary classification settings: *Spotted vs Others* (grouping Broken, Skin damaged, and Immature) and *Intact vs Others* (grouping Spotted, Broken, Skin damaged, and Immature). These scenarios reflect real-world challenges in the soybean processing pipeline, where the goal is often to rapidly identify and separate ideal grains from defective ones, even when the specific damage type is not required. Evaluating these configurations across all three networks helps assess the robustness and applicability of the proposed approach in practical automated systems.

A. Dataset Description

The soybean grain images are obtained from the public repository Mendeley Data under the dataset “Soybean Seeds” [17]. The labeling criteria follow the *Standard of Soybean Classification (GB1352-2009)*. The dataset consists of soybean seed images classified into five distinct categories based on their physical condition: *Broken*, *Immature*, *Intact*, *Skin damaged*, and *Spotted*. Figure 3 illustrates one example image corresponding to each of the five soybean classes.

Original images are captured at a resolution of 3072×2048 pixels. From these, 227×227 pixel PNG crops are extracted. To assess the effectiveness of the proposed methodology, we employed a balanced dataset comprising only 200 images from each class, resulting in a total of 1,000 samples. All images are in color, with a dark background and standardized lighting to minimize external variability.

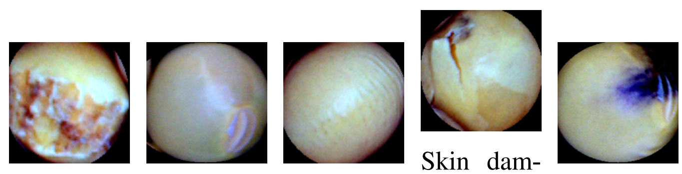

Broken | Immature | Intact | Skin damaged | Spotted

Fig. 3: Representative image samples for each soybean seed class [17].

The five categories present overlapping visual cues: *Broken* seeds are cracked or fragmented and may resemble partially *Skin damaged* or *Spotted* grains; under varying illumination; *Intact* seeds are generally regular and undamaged but may overlap with mildly *Immature* or *Skin damaged* cases; *Skin damaged* seeds exhibit abrasions or small cracks with severity-dependent variability; and *Spotted* seeds show dark spots that may be mistaken for *Skin damaged* when spot color or distribution is ambiguous.

This high intra- and inter-class variability presents a significant challenge for classification models, emphasizing the need for robust and discriminative representations.

B. Feature Vector Results

Each image yields a 50-dimensional descriptor (10 metrics $\times$ 5 graphs). Using the combined ANOVA and Mutual Information ranking, we select the top 25 discriminative features. Table I lists the selected features and their acronyms used in Fig. 4. Fig. 4 summarizes the normalized class-wise profiles of the selected features, highlighting that different graph views (color channels, texture, curvature) contribute complementary structural cues for discrimination.

TABLE I: List of the 25 selected features with their acronyms.

Acronym	Description
EWμ_Tex	Mean edge weights in the texture graph
EWμ_G	Mean edge weights in the green channel graph
AC_Tex	Average clustering in the texture graph
AWD_R	Weighted average degree in the red channel graph
ASP_G	Average shortest path in the green channel graph
EWμ_R	Mean edge weights in the red channel graph
CLμ_G	Mean closeness centrality in the green channel graph
AWD_G	Weighted average degree in the green channel graph
ASP_B	Average shortest path in the blue channel graph
EWσ_G	Standard deviation of edge weights in the green channel graph
AC_R	Average clustering in the red channel graph
EWμ_B	Mean edge weights in the blue channel graph
CLμ_B	Mean closeness centrality in the blue channel graph
AWD_Tex	Weighted average degree in the texture graph
AWD_B	Weighted average degree in the blue channel graph
CLμ_R	Mean closeness centrality in the red channel graph
EWσ_Tex	Standard deviation of edge weights in the texture graph
ASP_R	Average shortest path in the red channel graph
EWσ_R	Standard deviation of edge weights in the red channel graph
EWσ_B	Standard deviation of edge weights in the blue channel graph
WDσ_Tex	Weighted degree standard deviation in the texture graph
ASP_Tex	Average shortest path in the texture graph
AC_G	Average clustering in the green channel graph
WAss_Tex	Weighted assortativity in the texture graph
CLμ_Tex	Mean closeness centrality in the texture graph

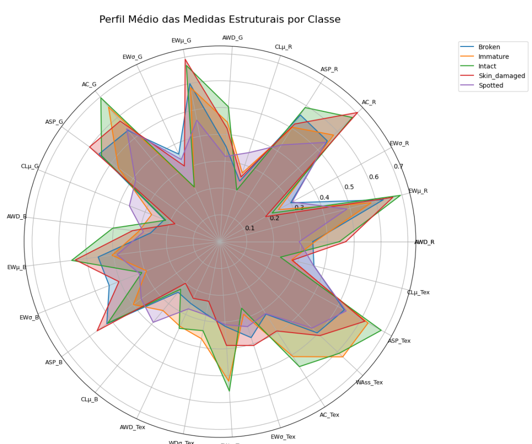

Fig. 4: Normalized average profile of the top 25 structural graph features from the total 50 features by class.

C. Classification Results

This section presents the performance of the classification models under three different scenarios: (i) classification with all five original classes; (ii) binary classification for *Spotted vs Others*; and (iii) binary classification for *Intact vs Others*. Each test has been conducted using both the image-only setup ("I") and a hybrid version that combines image features with graph-based structural measures ("I + G").

1) Five-Class Classification: Table II summarizes the results for the five-class scenario. EfficientNet achieves the highest accuracy when using image data alone. However, all three models (EfficientNet, InceptionV3, and ResNet50) show substantial performance gains when graph-based features are incorporated ("I+G"), outperforming their image-only configurations ("I").

TABLE II: Classification performance for all five classes.

Model	Setup	Acc.	F1-score	Prec. / Recall
ResNet50	I	0.7667	0.7646	0.7891 / 0.7667
	I + G	0.8081	0.8630	0.9468 / 0.8081
InceptionV3	I	0.6867	0.6810	0.7084 / 0.6867
	I + G	0.8687	0.8699	0.8713 / 0.8687
EfficientNet	I	0.7067	0.7057	0.7067 / 0.7007
	I + G	0.8687	0.9094	0.9646 / 0.8687

2) Binary Classification: Spotted vs Others: In real-world applications, the rapid and early separation of spotted grains from other types is crucial to prevent further contamination of healthy grains. In this scenario, again, the use of graph-based structural features led to substantial gains across all three architectures. InceptionV3 and EfficientNet achieved near-perfect performance when augmented with graph measures, as shown in Tab. III.

TABLE III: Binary classification results for *Spotted vs Others*.

Model	Setup	Acc.	F1-score	Prec. / Recall
ResNet50	I	0.9000	0.9050	0.9157 / 0.9000
	I + G	0.9367	0.9363	0.9436 / 0.9367
InceptionV3	I	0.9083	0.9015	0.9185 / 0.9083
	I + G	0.9873	0.9936	1.0000 / 0.9873
EfficientNet	I	0.9083	0.9102	0.9156 / 0.9083
	I + G	0.9747	0.9872	1.0000 / 0.9747

3) Binary Classification: Intact vs Others: In some cases, the focus is solely on collecting intact grains, with all other types being discarded. For the *Intact vs Others* scenario, all models benefited from the inclusion of graph-based features. EfficientNet once again outperforms the others in both setups, with its hybrid version ("I+G") achieving the highest scores, as shown in Tab. IV.

TABLE IV: Binary classification results for *Intact vs Others*.

Model	Setup	Acc.	F1-score	Prec. / Recall
ResNet50	I	0.9000	0.8966	0.8985 / 0.9000
	I + G	0.9192	0.9203	0.9224 / 0.9192
InceptionV3	I	0.9000	0.8995	0.8990 / 0.9000
	I + G	0.9495	0.9511	0.9552 / 0.9495
EfficientNet	I	0.9267	0.9248	0.9258 / 0.9267
	I + G	0.9697	0.9706	0.9742 / 0.9697

IV. Conclusions

This paper presented a graph-based framework for soybean seed quality assessment, in which images are segmented into superpixels, transformed into graphs encoding similarities in color, texture, and curvature, and summarized through compact structural descriptors. These graph-derived descriptors were evaluated in combination with CNN-based representations within a hybrid classification setting.

Experimental results on a five-class classification task, as well as two practical binary scenarios (Spotted vs Others and

Intact vs Others), demonstrate that incorporating graph-based descriptors consistently improves performance over image-only baselines across ResNet50, InceptionV3, and EfficientNet. Overall, the findings indicate that structural descriptors provide complementary information to convolutional representations, enhancing class discrimination, particularly in settings with limited training data.

Future work will explore several directions to further advance this framework. First, we will investigate localized and hierarchical subgraph descriptors to enable fine-grained, region-specific characterization of seed defects, potentially improving interpretability and supporting more precise damage quantification. Second, we plan to develop lightweight and optimized graph construction and inference strategies to enable real-time deployment in industrial inspection pipelines, including edge-device implementations. Third, integrating multimodal information, such as hyperspectral or thermal imaging—may further enhance the robustness of the descriptors under varying acquisition conditions. In addition, extending the framework to self-supervised or weakly supervised learning paradigms could reduce the reliance on annotated data while improving generalization. Finally, future studies will evaluate the transferability of the proposed approach across different crop species and defect types, aiming to establish a generalizable and scalable solution for automated seed quality assessment in practical agricultural settings.

Acknowledgements

This research was funded by São Paulo Research Foundation (FAPESP) by grant number 2019/07665-4 and 2024/15430-5, Brazilian National Council for Scientific and Technological Development (CNPq) by grant number 403307/2025-2, 406417/2022-9, 420212/2023-0 and 306788/2023-3, Minas Gerais Research Foundation – FAPEMIG (grant n. BDT-00010-25), Brazilian Federal Agency for Support and Evaluation of Graduate Education (CAPES), and National Natural Science Foundation of China (NSFC) by grant number W2412112.

References

[1] FAO - Food and Agriculture Organization, FAOSTAT - Crops and livestock products: Soybeans, available online: https://www.fao.org/faostat/en/#data/QCL (accessed on 4 June 2025) (2023).

[2] H. Pratap, G. Prasad, P. Agarwal, A. Bhardwaj, A. Mehra, S. Mathpati, Soynet: Deep learning approaches for automated soybean seed quality assessment, 2024, pp. 613–617.
URL https://api.semanticscholar.org/CorpusID:270397242

[3] I. A. M. Dioses, J. L. D. Jr, R. N. Aquino, C. G. Feliciano, J. B. Tababa, L. Hermosura, Soybean seed quality assessment classification using efficientnet b0 algorithm, 2025, pp. 144–149.
URL https://api.semanticscholar.org/CorpusID:277319548

[4] Z. Huang, R. Wang, Y. Cao, S. Zheng, Y. Teng, F. Wang, L. Wang, J. Du, Deep learning based soybean seed classification, Computers and Electronics in Agriculture 202 (2022) 107393. doi:https://doi.org/10.1016/j.compag.2022.107393.
URL https://www.sciencedirect.com/science/article/pii/S0168169922007013

[5] D. C. Santana, A. C. C. Seron, L. P. R. Teodoro, I. C. de Oliveira, C. A. da Silva Junior, F. H. R. Baio, C. C. B. F. Ítavo, L. C. V. Ítavo, P. E. Teodoro, Classification of soybean groups for grain yield and industrial traits using vnir-swir spectroscopy, Infrared Physics & Technology 139 (2024) 105326. doi:https://doi.org/10.1016/j.infrared.2024.105326.
URL https://www.sciencedirect.com/science/article/pii/S135044952400210X

[6] C. Liu, Y. Shen, F. Mu, H. Long, A. Bilal, X. Yu, Q. Dai, Detection of surface defects in soybean seeds based on improved yolov9, Scientific Reports 15 (2025).
URL https://api.semanticscholar.org/CorpusID:277739616

[7] L. C. Ribas, J. J. de Mesquita Sá Junior, A. Manzanera, O. M. Bruno, Learning graph representation with randomized neural network for dynamic texture classification, Applied Soft Computing 114 (2022) 108035. doi:https://doi.org/10.1016/j.asoc.2021.108035.
URL https://www.sciencedirect.com/science/article/pii/S1568494621009571

[8] J. Nie, L. Huang, C. Zheng, X. Lv, R. Wang, Cross-scale graph interaction network for semantic segmentation of remote sensing images, ACM Trans. Multimedia Comput. Commun. Appl. 19 (6) (May 2023). doi:10.1145/3558770.
URL https://doi.org/10.1145/3558770

[9] R. Achanta, A. Shaji, K. Smith, A. Lucchi, P. Fua, S. Süsstrunk, Slic superpixels compared to state-of-the-art superpixel methods, IEEE Transactions on Pattern Analysis and Machine Intelligence 34 (11) (2012) 2274–2282. doi:10.1109/TPAMI.2012.120.

[10] R. C. Gonzalez, R. E. Woods, Digital image processing, Prentice Hall, Upper Saddle River, N.J., 2008.

[11] H. Scharr, Optimal operators in digital image processing, 2000.
URL https://api.semanticscholar.org/CorpusID:28512423

[12] M. E. J. Newman, Networks: an introduction, Oxford University Press, Oxford; New York, 2010.

[13] L. d. F. Costa, F. A. Rodrigues, G. Travieso, P. R. Villas Boas, Characterization of complex networks: A survey of measurements, Advances in Physics 56 (1) (2007) 167–242. doi:10.1080/00018730601170527.
URL http://dx.doi.org/10.1080/00018730601170527

[14] K. He, X. Zhang, S. Ren, J. Sun, Deep residual learning for image recognition (2015). arXiv:1512.03385.
URL https://arxiv.org/abs/1512.03385

[15] C. Szegedy, V. Vanhoucke, S. Ioffe, J. Shlens, Z. Wojna, Rethinking the inception architecture for computer vision (2015). arXiv:1512.00567.
URL https://arxiv.org/abs/1512.00567

[16] M. Tan, Q. V. Le, Efficientnet: Rethinking model scaling for convolutional neural networks (2020). arXiv:1905.11946.
URL https://arxiv.org/abs/1905.11946

[17] Mendeley Data, Soybean seeds, [Dataset], Published on May 30, 2023 (2023). doi:10.17632/v6vzvfszj6.6.